Influence of the Dirac sea on proton electromagnetic knockout

James J. Kelly
Department of Physics, University of Maryland, College Park, MD 20742
(Dated: January 28, 2005)

We use the relativistic distorted-wave impulse approximation (RDWIA) to study the effects of negative-energy components of Dirac wave functions on the left-right asymmetry for $(e,e'p)$ reactions on ^{16}O with $0.2 \le Q^2 \le 0.8$ and ^{12}C with $0.6 \le Q^2 \le 1.8$ $(\mathrm{GeV}/c)^2$. Spinor distortion is more important for the bound state than for the ejectile and the net effect decreases with Q^2. Spinor distortion breaks Gordon equivalence and the data favor the CC2 operator with intermediate coupling to the sea. The left-right asymmetry for $Q^2 \lesssim 1.2$ $(\mathrm{GeV}/c)^2$ is described well by RDWIA calculations, but at $Q^2 = 1.8$ $(\mathrm{GeV}/c)^2$ the observed variation with missing momentum is flatter than predicted.

I. INTRODUCTION

One of the interesting features of nucleon electromagnetic knockout reactions is the sensitivity of some observables to negative-energy states in the Dirac sea. When a Dirac equation with scalar and vector potentials, S and V, is transformed to an equivalent Schrödinger equation, the effective spin-orbit potential is proportional to $S - V$. Within a nucleus, $S - V$ reduces the effective mass, thereby reducing the upper and enhancing the lower components of the Dirac wave function. Modification of the relationship between lower and upper components requires admixture of negative-energy Dirac states. Observables sensitive to coupling between lower and upper components can then reveal the role of negative-energy states.

Several recent papers have investigated the effects of spinor distortion in some detail [1, 2, 3, 4, 5, 6, 7]. In this short paper we will explore the Q^2 dependence of such effects using data for ^{16}O and ^{12}C$(e,e'p)$ in quasiperpendicular kinematics for Q^2 between about 0.2 and 1.8 $(\mathrm{GeV}/c)^2$. The data for ^{16}O have already been analyzed in considerable detail and the enhancement of the left-right asymmetry for $Q^2 = 0.8$ $(\mathrm{GeV}/c)^2$ has been interpreted as evidence for spinor distortion [8, 9]. Here we use the availability of both $1p_{3/2}$ and $1p_{1/2}$ magnetic substates to illustrate the sensitivity to several important aspects of spinor distortion. The recent ^{12}C$(e,e'p)$ data from Dutta [10] reaches larger Q^2 but were acquired to study nuclear transparency and were analyzed using either nonrelativistic or factorized calculations that omit spinor distortion. Here we use relativistic distorted-wave calculations to show that the left-right asymmetry in the reduced cross section for $Q^2 = 0.6$, 1.2, and 1.8 $(\mathrm{GeV}/c)^2$ is sensitive to spinor distortion also. We consider both semi-inclusive data and bins centered upon the $1p_{3/2}$ and $1s_{1/2}$ shells.

The model is described briefly in Sec. II. Data for ^{16}O and ^{12}C are examined in Secs. III A and III B, respectively. Our conclusions are summarized in Sec. IV.

II. MODEL

In this section we outline a series of approximations to the relativistic distorted-wave impulse approximation (RDWIA) that facilitate exploration of the effects of the Dirac sea and comparisons with nonrelativistic approaches (NRDWIA). Further details may be found in Ref. [9]. All calculations treat electron distortion in the q_{eff} approximation and use MMD form factors [11] and Coulomb gauge. Most calculations use the CC2 current operator unless noted otherwise. We consider Dirac-Hartree wave functions from the original Horowitz and Serot (HS) analysis [12] and NLSH wave functions from Sharma *et al.* [13]. Optical potentials for Dirac phenomenology were taken from the global analysis by Cooper *et al.* [14].

In RDWIA a nuclear matrix element of the single-nucleon electromagnetic current for the $A(e,e'N)B$ reaction takes the form

$$\mathcal{J}^\mu = \int d^3r \, \exp(i\boldsymbol{t}\cdot\boldsymbol{r}) \langle \Psi^{(-)}(\boldsymbol{p}',\boldsymbol{r}) | \gamma^0 \Gamma^\mu(\boldsymbol{p}',\boldsymbol{p}'-\boldsymbol{q}) | \Phi(\boldsymbol{r}) \rangle \tag{1}$$

where Γ^μ is the vertex function, $\boldsymbol{q}$ is the momentum transfer, $\boldsymbol{p}'$ is the ejectile momentum, and $\boldsymbol{t} = E_B\boldsymbol{q}/W$ is the recoil-corrected momentum transfer. The overlap Φ between initial and final nuclear states is often

called the bound-state wave function and includes the spectroscopic factor. According to standard distorted-wave theory [15, 16], the wave function $\Psi^{(-)}$ appears with incoming boundary conditions corresponding to incoming spherical waves in open channels of the $N+B$ system with an outgoing plane wave normalized to unit flux and is related to standard scattering wave functions,$\Psi^{(+)}$, by time reversal. Both wave functions are assumed to satisfy local single-nucleon Dirac equations of the form

$$[\boldsymbol{\alpha}\cdot\boldsymbol{p}+\beta(m+S_b)+(V_b-E_b)]\,\Phi \;=\; 0 \tag{2a}$$

$$[\boldsymbol{\alpha}\cdot\boldsymbol{p}+\beta(m+S_c)+(V_c-E_c)]\,\Psi^{(+)} \;=\; 0 \tag{2b}$$

where Φ and Ψ are four-component Dirac spinors, S and V are scalar and vector potentials, and the subscripts b and c distinguish between bound (initial) and continuum (final) states.

The bound-state spinor takes the form

$$\Phi_{\kappa m}(\mathbf{r}) = \begin{pmatrix} f_\kappa(r)\mathcal{Y}_{\kappa m}(\hat{r}) \\ ig_{-\kappa}(r)\mathcal{Y}_{-\kappa m}(\hat{r}) \end{pmatrix} \tag{3}$$

where

$$\mathcal{Y}_{\kappa m}(\hat{r}) = \sum_{s,m_s} \langle \begin{smallmatrix} \ell & \frac{1}{2} \\ \nu & m_s \end{smallmatrix} | \begin{smallmatrix} j \\ m \end{smallmatrix} \rangle Y_{\ell\nu}(\hat{r})\chi_{m_s} \tag{4}$$

is the spin spherical harmonic and where the orbital and total angular momenta are given by

$$\ell \;=\; S_\kappa(\kappa+\frac{1}{2})-\frac{1}{2} \tag{5a}$$

$$j \;=\; S_\kappa\kappa-\frac{1}{2} \tag{5b}$$

with $S_\kappa = sign(\kappa)$. The momentum distribution is then

$$\rho(p) = \frac{1}{2\pi^2}\left(|\tilde{f}_\kappa(p)|^2+|\tilde{g}_\kappa(p)|^2\right) \tag{6}$$

where

$$\tilde{f}_\kappa(p) \;=\; \int dr\; r^2 j_\ell(pr) f_\kappa(r) \tag{7a}$$

$$\tilde{g}_{-\kappa}(p) \;=\; \int dr\; r^2 j_{\ell'}(pr) g_{-\kappa}(r) \tag{7b}$$

Similarly, the ejectile distorted wave is represented by

$$\Psi(\mathbf{p},\mathbf{r}) = \sqrt{\frac{E_c+m}{2E_c}}\begin{pmatrix} \psi(\mathbf{r}) \\ \zeta(\mathbf{r}) \end{pmatrix} \tag{8}$$

where ψ and ζ are two-component Pauli spinors and the boundary conditions are suppressed.

It is often convenient to transform the two coupled first-order radial Dirac equations into a single second-order equation

$$\left[\nabla^2+k^2-2\mu\left(U^C+U^{LS}\boldsymbol{L}\cdot\boldsymbol{\sigma}\right)\right]\xi = 0 \tag{9}$$

where ξ is a two-component Pauli spinor [17, 18, 19]. Here k is the relativistic wave number, μ is the nucleon mass for the bound state or the relativistic reduced energy for the scattering state, and U^C and U^{LS} are central and spin-orbit potentials. The corresponding Dirac wave functions are then given by

$$\Phi \;=\; \Omega_b\xi_b \tag{10a}$$

$$\Psi \;=\; \Omega_c\xi_c \tag{10b}$$

where

$$\Omega(\boldsymbol{p},r) = \begin{pmatrix} 1 \\ \frac{\boldsymbol{\sigma}\cdot\boldsymbol{p}}{(E+m)D(r)} \end{pmatrix} D^{1/2}(r) \tag{11}$$

is a spinor-distortion operator based upon relativistic effective mass

$$D(r) = 1 + \frac{S(r) - V(r)}{E + M} \tag{12}$$

in the presence of Dirac scalar and vector potentials, S and V. Therefore, the direct Pauli reduction method [3, 20] is based upon a 2×2 current operator of the form

$$J^{\mu}(\boldsymbol{p}', \boldsymbol{p}) = \tilde{\Omega}_c(\boldsymbol{p}', r)\gamma^0\Gamma^{\mu}\Omega_b(\boldsymbol{p}, r) \tag{13}$$

that acts between the Pauli spinors for the relativized Schrödinger equations — the lower components of the original Dirac spinors have been incorporated within the operator. Note that the transpose of the ejectile spinor distortion appears instead of its Hermitian conjugate because of its incoming boundary conditions. Thus, one can identify two primary relativistic effects. First, the Darwin potential $D(r)$ reduces the interior wave function and generally has a narrowing effect upon the momentum distribution. Although the net effect is to increase spectroscopic factors fit to missing momentum distributions, such effects are similar to those of Perey nonlocality factors often used in nonrelativistic models [21]. Second, the presence of Dirac potentials produces dynamical enhancement of the lower components. Some observables, such as A_{LT}, are sensitive to this uniquely relativistic effect through coupling between upper and lower components mediated by the electromagnetic current operator.

Several approximations provide useful insight into the roles of various relativistic effects. The effective momentum approximation (EMA) replaces the momentum operators that appear in spinor-distortion operators by asymptotic kinematics. Thus, the the initial momentum of the struck nucleon, $\boldsymbol{p}_b$, is identified with the asymptotic missing momentum $\boldsymbol{p}_m = \boldsymbol{p}' - \boldsymbol{q}$. The so-called noSV approximation then uses

$$\Omega(\boldsymbol{p}, r) \longrightarrow \begin{pmatrix} 1 \\ \frac{\boldsymbol{\sigma}\cdot\boldsymbol{p}}{E+m} \end{pmatrix} D^{1/2}(r) \tag{14}$$

to eliminate the dynamical enhancement of lower components. Note, however, that the common Darwin factor is retained because it has an important effect upon the momentum distribution. The combined EMA-noSV approximation [3, 19] has the advantage that it can be used with two-component nonrelativistic wavefunctions without using p/m expansions of the current operator. Such wave functions are usually represented by

$$\Phi(r) = P_b(r)^{1/2}\xi_b(r) \tag{15}$$

where

$$P_b(r) = \left(1 - \frac{\mu_b\beta_{\rm NL}^2}{2}U_b^C(r)\right)^{-1} \tag{16}$$

is a Perey nonlocality factor [22] based upon the central binding potential and where $\beta_{\rm NL} \sim 0.85$ fm. Thus, if one replaces the Darwin potential in the spinor distortion factor by the Perey factor, the EMA-noSV approach becomes practically identical to a conventional NRDWIA calculation. Furthermore, only the ejectile spin-orbit potential violates factorization of RDWIA calculations based upon the EMA-noSV approximation. A more detailed discussion of factorization in these approximations has been given by Refs. [1, 6].

The EMA-SV approximation introduced in Ref. [3] also replaces momentum operators by asymptotic kinematics but retains the scalar and vector potentials in the spinor-distortion operator, thereby providing an estimate of the effects of dynamical enhancement of the lower components of the Dirac spinors by the mean field that is faster and numerically simpler than a full RDWIA calculation. When using potentials defined for the Schrödinger equation, the Darwin potential can be obtained from the spin-orbit potential according to [23]

$$D(r) = \exp\left(2\mu\int_r^{\infty} dr' r'\, U^{LS}(r')\right) \tag{17}$$

These representations of the Darwin potential are equivalent for RDWIA calculations for which U^C and U^{LS} are defined in terms of S and V but are not necessarily equivalent for NRDWIA calculations where

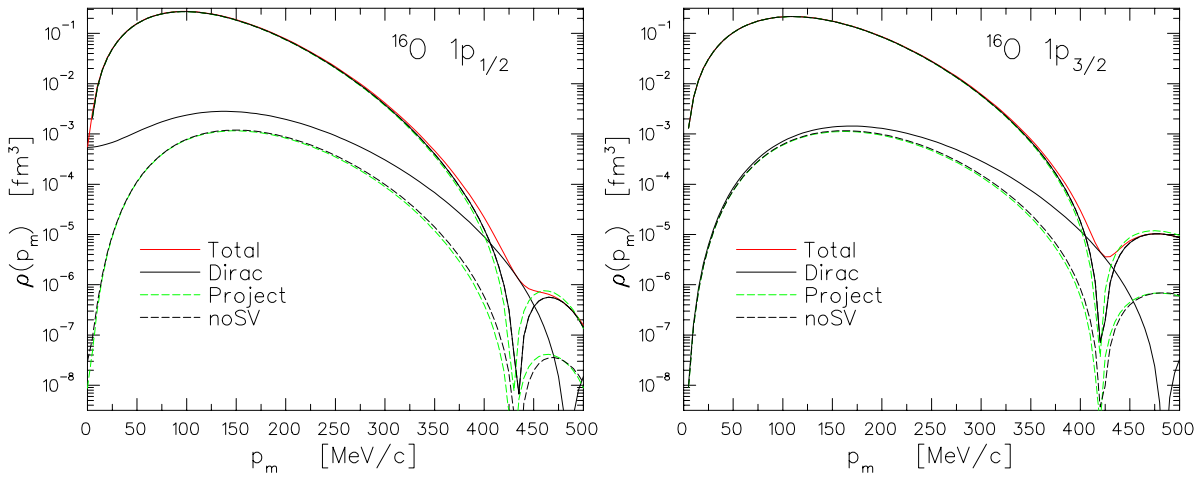

FIG. 1: (Color online) Missing momentum distribution for $^{16}\mathrm{O}(e,e'p)(1p)^{-1}$. The solid red curves show the total momentum distribution and solid black the contributions of upper and lower components of the Dirac wave functions. The green dashed curves show the effect of projection on positive-energy states while black dashed curves show the noSV approximation. NLSH wave functions were used for this exercise.

the central and spin-orbit potentials are optimized independently. Nevertheless, it is sometimes instructive to perform EMA-SV calculations using Woods-Saxon wave functions fitted to $(e,e'p)$ data using NRDWIA methods. However, the difference between $P(r)$ based upon U^C and $D(r)$ based upon U^{LS} can affect the momentum distribution.

The role of negative-energy contributions of the Dirac sea can be evaluated by applying the projection operator [5, 7]

$$\Lambda_+(\boldsymbol{p}) = \frac{m + \not{p}}{2m} \tag{18}$$

to Φ, Ψ, or both. Figure 1 illustrates the effect of positive-energy projection upon the momentum distributions for $1p$-shell knockout from ^{16}O. The contribution of lower components is generally small, except near the diffraction minima of the upper component, but can still be very important for observables, such as A_{LT} that emphasize interference between lower and upper components. The negative-energy contribution is practically negligible for the upper component, but can be appreciable for the lower component. The negative-energy contribution to the lower component of the $1p_{3/2}$ state is small for low p_m but increases with p_m, becoming dominant near the diffraction minimum. By contrast, the negative-energy contribution to the lower component of the $1p_{1/2}$ state is relatively strong for all p_m — in fact, it dominates for small p_m because it has $\ell' = \ell - 1 = 0$ for $j = \ell - 1/2$. For both states we find that the noSV approximation is very similar, but not quite identical, to the result of positive-energy projection. Therefore, we expect the noSV approximation to provide an accurate but much faster estimate of the effect of positive-energy projection, at least for the bound state.

III. RESULTS

A. $^{16}\mathrm{O}(e,e'p)$

The left-right asymmetry in differential cross section is defined by

$$A_{LT} = \frac{\sigma(\phi = 0) - \sigma(\phi = \pi)}{\sigma(\phi = 0) + \sigma(\phi = \pi)} \tag{19}$$

where the subscript recognizes that this quantity is closely related to the longitudinal-transverse response function and where the azimuthal angle $\phi = 0$ corresponds to an ejectile momentum in the electron scattering

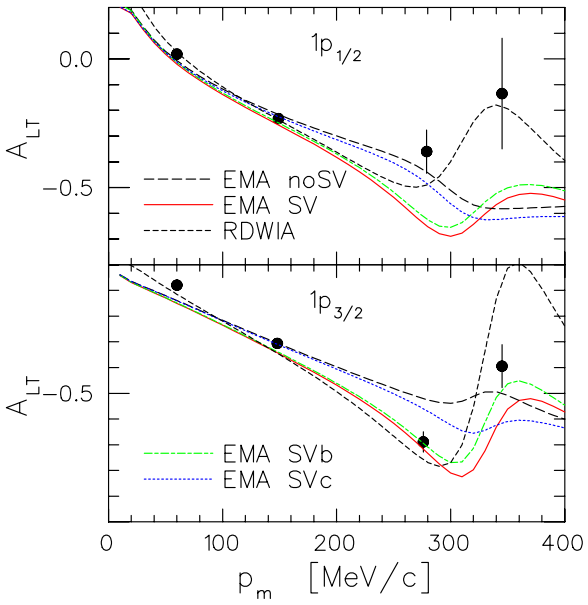

FIG. 2: (Color online) Left-right asymmetry for ^{16}O$(e,e'p)$ at $Q^2 = 0.8$ (GeV/c)^2. Black dashed and red solid curves compare EMA-noSV and EMA-SV calculations, while green dash-dotted and blue dotted illustrate the effects of spinor distortion on bound and ejectile wave functions, respectively. Finally, the black short-dashed curves show full RDWIA calculations.

plane between the beam direction and the momentum transfer. This quantity is especially sensitive to spinor distortion and has the advantages that it is independent of the spectroscopic factor and for modest missing momentum is relatively insensitive to both the momentum distribution for the bound state and the optical potential for the ejectile.

Figure 2 examines the effect of spinor distortion for the bound and/or ejectile wave functions in the context of EMA. Except for small spin-orbit effects in the final-state, the EMA-noSV approximation nearly factorizes so that A_{LT} is similar to that for a free but moving nucleon. Spinor distortion for the ejectile has relatively little effect at large Q^2 but is quite important for the bound state wave function, strengthening A_{LT} for $p_m \lesssim 300$ MeV/c and producing pronounced oscillations at larger p_m that can be attributed to the breakdown of factorization. Comparison between the black short-dashed and solid red curves shows that EMA calculations are similar to those of the full RDWIA for $p_m \lesssim 250$ MeV/c, but tend to underestimate the oscillations for larger p_m.

Figure 3 examines the sensitivity of A_{LT} to the contribution of negative-energy states. The differences between the EMA-noSV curves and the noSV curves show that errors due to the effective momentum approximation can be appreciable even without spinor distortion. The similarity between noSV curves (without EMA) and those that project upon positive-energy states shows that the dominant effect of spinor distortion arises from coupling to the Dirac sea. The fact that the noSV approximation is similar to positive-energy projection was also observed in Fig. 1 for the momentum distribution. Positive-energy projection is also shown separately for the bound state (green dash-dotted curves) and for the ejectile (magneta dotted curves). Thus, comparing the curves labelled project b or project c with those labelled RDWIA, we observe that the sensitivity of A_{LT} to spinor distortion is greater for the bound state than for the ejectile and that positive energy projection is similar to the noSV approximation for both. The difference between projected and RDWIA calculations shows that the sensitivity to the Dirac sea is greater for the $1p_{1/2}$ state, especially for small p_m. That effect is subtle, but the low p_m data do support the sea contribution. Clearly it would be desirable to obtain more complete data for $p_m \lesssim 300$ MeV/c where the single-nucleon knockout mechanism is most reliable.

Figure 4 surveys the Q^2 dependence of A_{LT} for ^{16}O$(e,e'p)$. The data for $Q^2 = 0.2$ are from Spaltro *et al.* [24] while those for $Q^2 = 0.3$ (GeV/c)^2 are from Chinitz *et al.* [25]. These calculations use NLSH wave functions, EDAD1 optical potential, CC2 current operator, and Coulomb gauge. The experimental asymmetry for the $1p_{1/2}$ state is slightly stronger than obtained from positive-energy states alone and is in

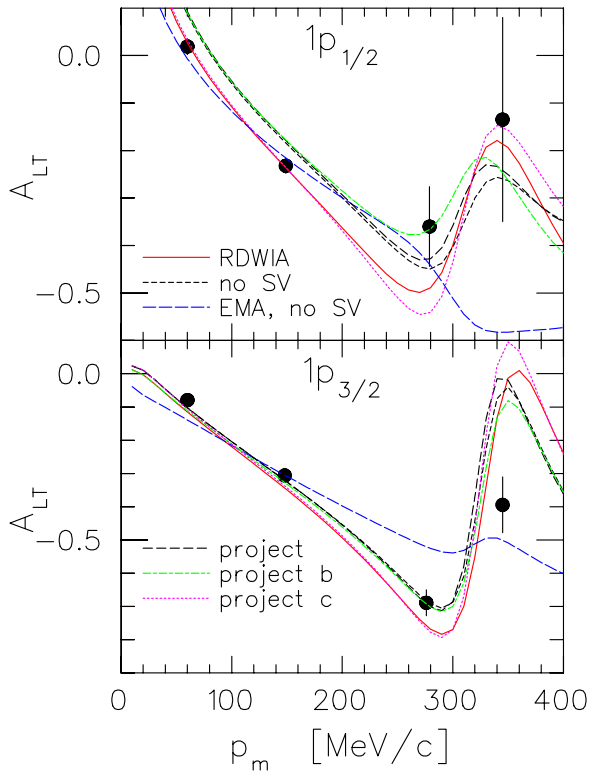

FIG. 3: (Color online) Left-right asymmetry for ^{16}O$(e,e'p)$ at $Q^2 = 0.8$ (GeV/c)^2. The red solid curves show RDWIA, black short-dashed curves show noSV, blue long-dashed curves show EMA-noSV calculations. Calculations with positive-energy projection are shown as green dash-dotted curves for the bound nucleon, magenta dotted curves for the ejectile, or black dashed curves for both.

good agreement with the full RDWIA calculations. The sensitivity to negative-energy states is smaller for the $1p_{3/2}$ state, but the RDWIA calculations are still in good agreement with the data for $Q^2 = 0.3$ and 0.8 (GeV/c)^2. Although the calculations do not describe the $1p_{3/2}$ A_{LT} data for $Q^2 = 0.3$ (GeV/c)^2 well, we are somewhat skeptical of the reliability of that particular data set because Fissum *et al.* [9] showed that there is an enhancement of this cross section for $50 < p_m < 120$ MeV/c that cannot be reproduced by any of the many variations of the RDWIA model that were considered. Therefore, we judge the overall agreement between RDWIA calculations and the A_{LT} data for ^{16}O$(e,e'p)$ to support the participation of the Dirac sea in the bound-state wave function. However, the data are not as precise nor the p_m coverage as complete as we would like.

Finally, Fig. 5 shows the sensitivity of A_{LT} to the Gordon ambiguity in the single-nucleon current operator. All three operators are equivalent when the relationship between lower and upper components is the same as for free nucleons, as in the EMA-noSV approximation, but spinor distortion breaks that equivalence. Thus, CC1 shows the greatest and CC3 the least sensitivity to spinor distortion. This sensitivity is especially large for the $1p_{1/2}$ state and decreases as Q^2 increases. It is interesting to observe that dynamical relativistic effects are most important at low Q^2. The coupling of the ejectile to the Dirac sea is driven by $(S-V)/(E+m)$, which decreases as $E \sim Q^2/2m$ increases. However, there is as yet no fundamental theory that distinguishes between Gordon-equivalent forms of the single-nucleon current. The available data for ^{16}O$(e,e'p)$ favor the intermediate CC2 current operator.

B. ^{12}C$(e,e'p)$

Dutta *et al.* [10] measured the reduced cross section for ^{12}C$(e,e'p)$ in quasiperpendicular kinematics at $Q^2 = 0.6$, 1.2, and 1.8 (GeV/c)^2 . Although two beam energies are available for the first and third sets, we

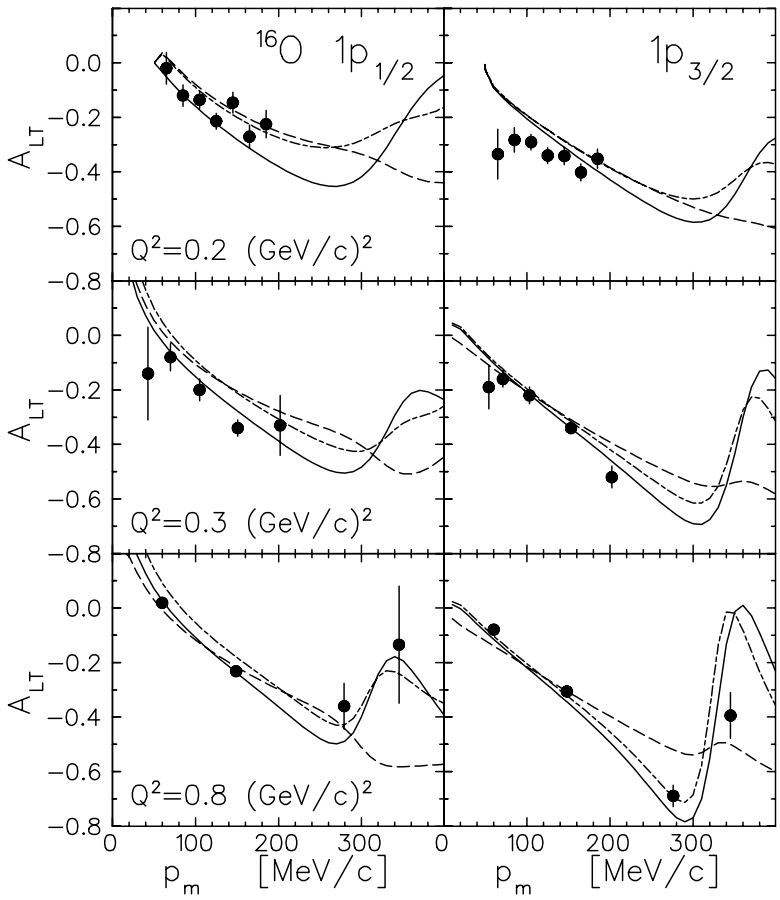

FIG. 4: Dashed curves show EMA-noSV, solid curves RDWIA, and dash-dotted curves use positive-energy projection for ^{16}O$(e,e'p)$.

consider only the higher energy and more forward electron-scattering angle because the more complete coverage of the ejectile angle under those conditions provides the left-right asymmetry. The left-right asymmetry for reduced cross section is defined

$$a_{LT} = \frac{\sigma_{\rm red}(\phi=0) - \sigma_{\rm red}(\phi=\pi)}{\sigma_{\rm red}(\phi=0) + \sigma_{\rm red}(\phi=\pi)} \tag{20}$$

and is small in PWIA because the intrinsic left-right asymmetry of e-p elastic scattering is removed by reduction of the differential cross section. Note that we use a lower-case a for the asymmetry in reduced cross section and upper-case A for the corresponding asymmetry in differential cross section.

The data were presented in three bins: the lower bin with $15 \le E_m \le 25$ MeV is dominated by the $1p_{3/2}$ contribution, the upper bin with $30 \le E_m \le 50$ MeV emphasizes the $1s_{1/2}$ contribution, while the semi-inclusive bin with $10 \le E_m \le 80$ MeV also includes a significant continuum. For the present purposes it is sufficient to treat the lower bin as pure $1p_{3/2}$, the upper bin as pure $1s_{1/2}$, and the inclusive bin as an incoherent mixture based upon the independent particle shell model (IPSM). The calculations for each orbital are based upon Dirac-Hartree wave functions and neglect the spreading with respect to missing energy. We apply the same parametrization to the inclusive bin because we do not have a detailed calculation of the continuum. Although neither of the two narrow bins is pure and the inclusive bin includes continuum contributions, a_{LT} for single-nucleon knockout is rather insensitive to small deviations with respect to IPSM and we are more interested here in sensitivities to various aspects of the reaction model than in optimization of the spectral function. A subsequent paper [26] will analyze the spectroscopic factors and nuclear transparency for these data.

The sensitivity of a_{LT} to the treatment of lower components is examined in Fig. 6. The dashed curves show that the left-right asymmetry for EMA-noSV is very similar to that for RPWIA because the relationship

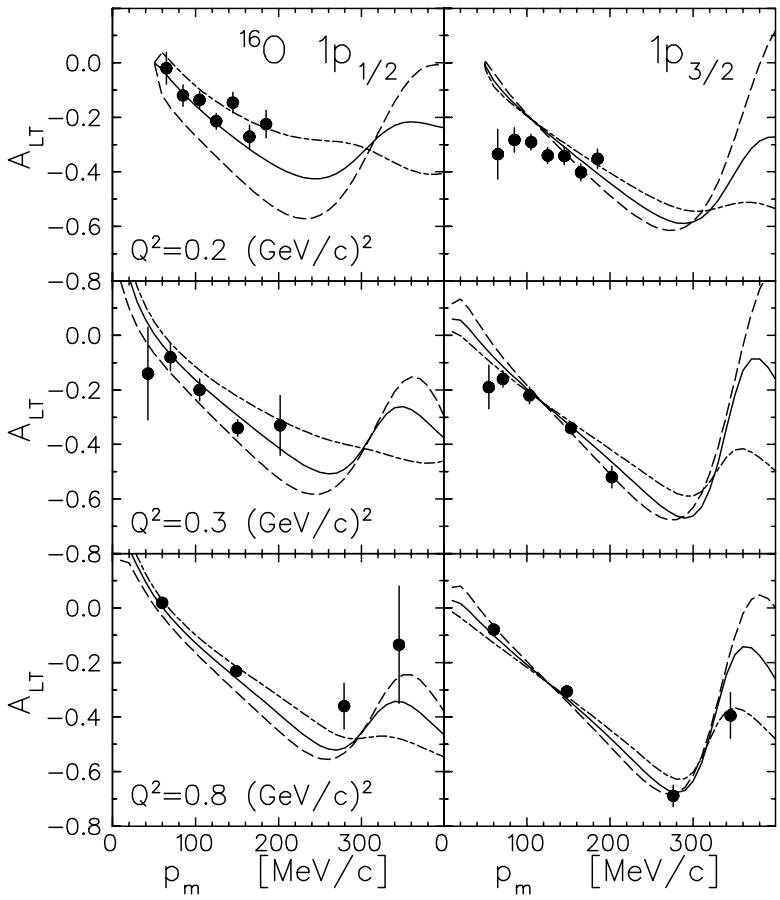

FIG. 5: Dashed, solid, and dash-dotted curves show RDWIA calculations for ^{16}O$(e, e'p)$ using the CC1, CC2, and CC3 current operators, respectively.

between lower and upper components is based upon asymptotic kinematics for free nucleons. The very small variations of a_{LT} are due to distortion effects that do not factorize completely. The dash-dotted curves use wave functions projected onto positive-energy states that produce similar but somewhat smaller asymmetries than the full calculation shown by solid curves. The small differences between those curves is indicative of the contribution of the Dirac sea, whose importance decreases slowly with increasing Q^2.

The sensitivity of RDWIA calculations to the Gordon ambiguity in the single-nucleon current operator is displayed in Fig. 7. Clearly, the CC1 operator is most and the CC3 operator is least sensitive to dynamical enhancement of the lower component of Dirac wave functions. This sensitivity decreases fairly rapidly as Q^2 increases and has nearly disappeared by 1.8 $(\mathrm{GeV}/c)^2$. The data for lower Q^2 appear to favor the CC2 operator with intermediate sensitivity to this effect.

The sensitivity to the overlap function is illustrated in Fig. 8. The calculations shown for the $1p$ and $1s$ bins assume pure $1p_{3/2}$ and $1s_{1/2}$ wave functions while those for the inclusive bin assume full occupancy for both shells. The results for the two relativistic wave functions, NLSH and HS, are practically identical but the Woods-Saxon wave functions fitted by van der Steenhoven *et al.* [27, 28] to data from NIKHEF give significantly different results: the turnaround occurs earlier and a_{LT} is stronger, especially for the $1s$ state. The data generally favor the relativistic bound-state wave functions, although the $1s$ distributions tend to be flatter than those calculations as Q^2 increases. To obtain relativistic calculations using Woods-Saxon wave functions, the Perey factor was replaced by a Darwin factor computed from the spin-orbit potential according to Eq. (17). The same Darwin potential was also used for dynamical enhancement of the lower component of the Dirac spinor according to Eq. (11). Recognizing that EMA-noSV calculations are quite insensitive to the upper components because the violation of factorization by ejectile distortion is small, the main difference between a_{LT} calculations using relativistic or nonrelativistic wave functions can be attributed to

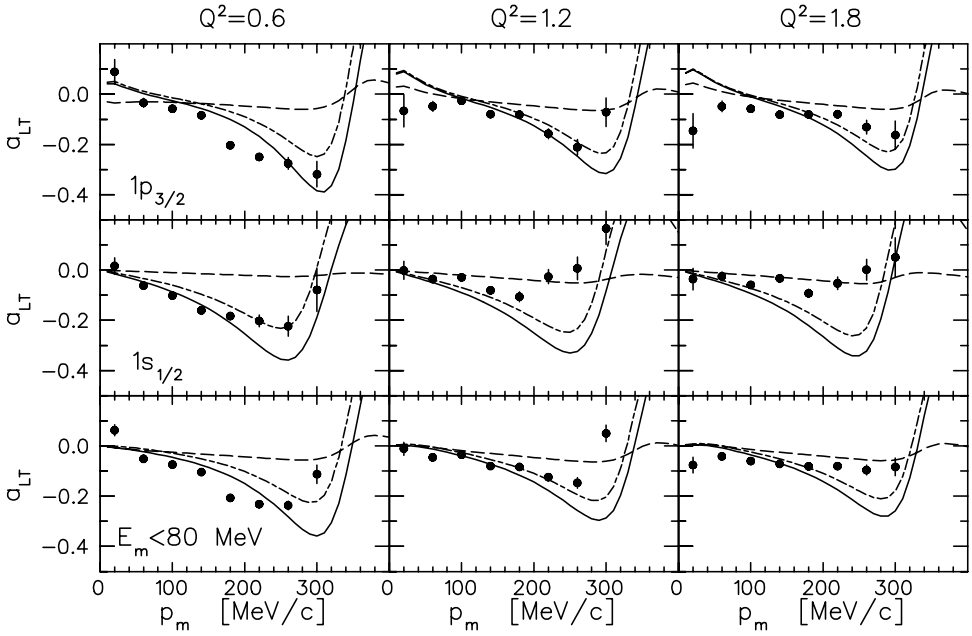

FIG. 6: Dashed curves show EMA-noSV, solid curves RDWIA, and dash-dotted curves use positive-energy projection for ^{12}C$(e,e'p)$. The top row shows data for $15 \leq E_m \leq 25$ MeV, the middle row for $30 \leq E_m \leq 50$ MeV, and the bottom row for $10 \leq E_m \leq 80$ MeV.

the difference between the $S-V$ potentials. Although the $S-V$ potential for the bound state can be obtained from the spin-orbit potential in principle, in practice this quantity is poorly constrained by nonrelativistic $(e,e'p)$ calculations and is usually chosen somewhat arbitrarily. An advantage of the Dirac-Hartree approach is that the Darwin potential emerges naturally during the optimization of the binding energy.

Figure 9 shows that a_{LT} for $p_m \lesssim 250$ MeV/c is rather insensitive to the choice of optical potential. Similar results were obtained using folding-model potentials based upon the EEI or IA2 interactions [29]. Therefore, a_{LT} is more sensitive to the properties of the binding than the distorting potentials. Slight shifts of the distorted momentum distribution produce some sensitivity at larger p_m to details of the optical potential, but there one might expect other effects, such as two-body currents or channel coupling, to contribute also.

RDWIA calculations describe the a_{LT} data for $Q^2 \lesssim 1.2$ (GeV/c)^2 relatively well, but the data for $Q^2 = 1.8$ (GeV/c)^2 show less variation with p_m than predicted. The bin centered upon the s-shell also has a flatter p_m distribution for $Q^2 = 1.2$ (GeV/c)^2. The flattening of a_{LT} for s-shell and inclusive bins is probably due to continuum contributions that dilute the signal from single-nucleon knockout — although we do not have detailed calculations for the continuum, there is little reason to expect multinucleon knockout to retain the characteristic left-right asymmetry of single-nucleon knockout. However, continuum contamination of the p-shell bin should be very small because it lies below the two-nucleon emission threshold. One possibility is that the ejectile spin-orbit potential may be too strong for $T_p \sim 900$ MeV because analyzing power data for proton elastic scattering are scarce near the upper limit of the energy range used by Cooper *et al.* [14]. Alternatively, two-body currents may become important.

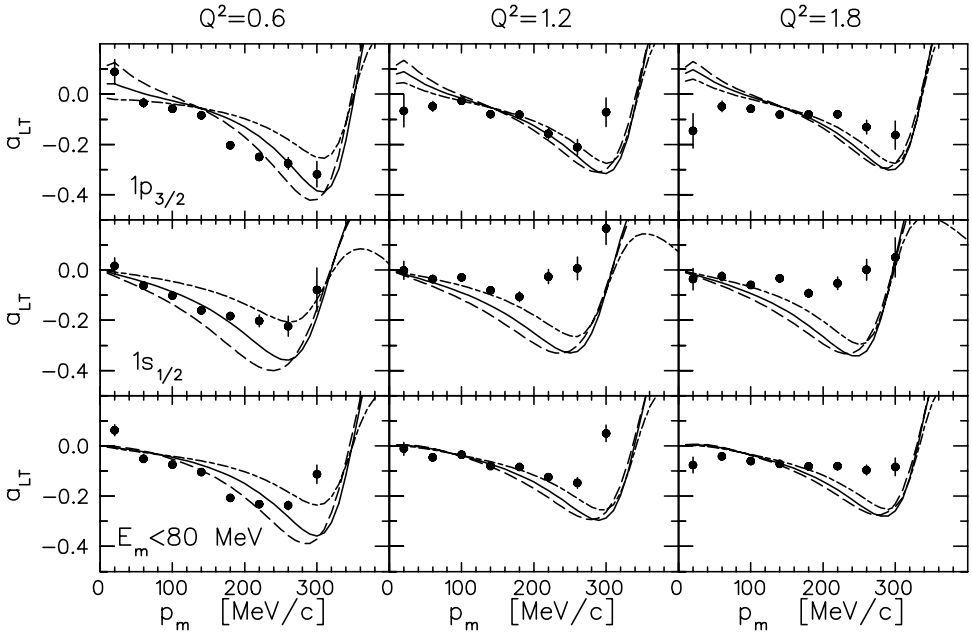

FIG. 7: Dashed, solid, and dash-dotted curves show ^{12}C$(e,e'p)$ calculations using the CC1, CC2, and CC3 current operators. All use NLSH wave functions, EDAD1 optical optical potentials, and Coulomb gauge. The top row shows data for $15 \leq E_m \leq 25$ MeV, the middle row for $30 \leq E_m \leq 50$ MeV, and the bottom row for $10 \leq E_m \leq 80$ MeV.

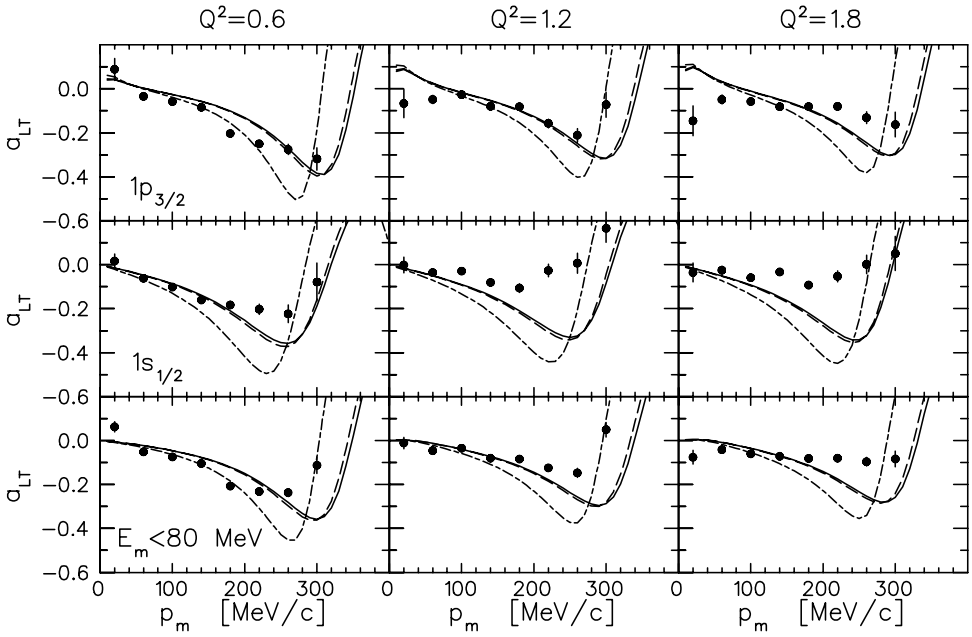

FIG. 8: Solid, dashed and dash-dotted curves show ^{12}C$(e,e'p)$ calculations using NLSH, HS, and NIKHEF wave functions. All use the CC2 current operator, Coulomb gauge, and EDAD1 optical potentials.

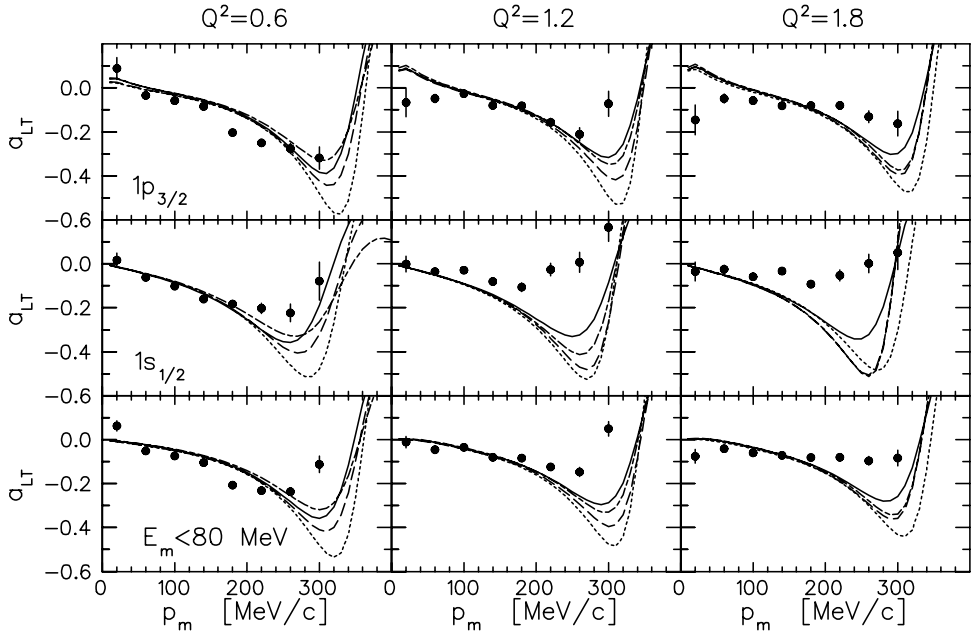

FIG. 9: Dotted, solid, dashed and dash-dotted curves show ^{12}C$(e,e'p)$ calculations using the EDAIC, EDAD1, EDAD2, and EDAD3 optical potentials. All use NLSH wave functions, CC2 current operator, and Coulomb gauge.

IV. SUMMARY AND CONCLUSIONS

The most important difference between relativistic and nonrelativistic DWIA calculations of single-nucleon electromagnetic knockout is spinor distortion: the enhancement of lower components of Dirac spinors by the nuclear spin-orbit potential or, equivalently, the difference $S - V$ between scalar and vector potentials. The left-right cross section asymmetry for quasiperpendicular kinematics is especially sensitive to distortion of the bound-state spinor. We have used data for proton knockout from ^{16}O and ^{12}C to evaluate the sensitivity of the left-right asymmetry to various aspects of the RDWIA for Q^2 between about 0.2 and 1.8 $(\mathrm{GeV}/c)^2$. We find:

- Negative-energy contributions are most important for $j < \ell$, especially when $\ell = 1$ permits negative-energy contributions for $p_m = 0$. The $1p_{1/2}$ data for $^{16}\mathrm{O}(e, e'p)$ are described significantly better by full RDWIA calculations than by either EMA or positive-energy projection. The noSV approximation is very similar to projection upon positive-energy states.
- The left-right asymmetry is more sensitive to the bound-state spin-orbit potential than to variations of the optical potential.
- Among the most common Gordon-equivalent current operators, CC1 has the most and CC3 the least sensitivity to spinor distortion. This sensitivity tends to decrease as Q^2 increases and is greater for $1p_{1/2}$ than for $1p_{3/2}$ proton knockout. The data for both ^{16}O and ^{12}C generally favor the intermediate choice, CC2.
- The left-right asymmetry for $^{12}\mathrm{C}(e, e'p)$ with $0.6 < Q^2 < 1.8$ $(\mathrm{GeV}/c)^2$ is described fairly well by RDWIA calculations, but the data become flatter than the calculations as Q^2 increases, especially for the $1s$ state. This effect for the $1p$ state might indicate that the spin-orbit potential in global optical potentials from Dirac phenomenology is somewhat too strong for $T_p > 600$ MeV. The more pronounced flattening for the $1s$ state might indicate greater contamination by multinucleon continuum.

Acknowledgments

We thank Dr. Dutta for tables of the a_{LT} data, Dr. Udías for tables of the NLSH and HS wave functions, and Dr. Lapikás for the parameters of the NIKHEF wave functions. The support of the U.S. National Science Foundation under grant PHY-0140010 is gratefully acknowledged.

[1] J. A. Caballero, T. W. Donnelly, E. M. de Guerro, and J. M. Udías, Nucl. Phys. **A632**, 323 (1998).
[2] J. A. Caballero, T. W. Donnelly, E. M. de Guerro, and J. M. Udías, Nucl. Phys. **A643**, 189 (1998).
[3] J. J. Kelly, Phys. Rev. **C 60**, 044609 (1999).
[4] J. M. Udías, J. A. Caballero, E. M. de Guerra, J. E. Amaro, and T. W. Donnelly, Phys. Rev. Lett. **83**, 5451 (1999).
[5] J. M. Udías, J. A. Caballero, E. M. de Guerra, J. R. Vignote, and A. Escuderos, Phys. Rev. **C 64**, 024616 (2001).
[6] J. R. Vignote, M. C. Martinez, J. A. Caballero, E. M. de Guerra, and J. M. Udias, Phys. Rev. **C 70**, 044608 (2004).
[7] M. C. Martínez, J. R. Vignote, J. A. Caballero, T. W. Donnelly, E. M. de Guerra, and J. M. Udías, Phys. Rev. **C 69**, 034604 (2004).
[8] J. Gao *et al.*, Phys. Rev. Lett. **84**, 3265 (2000).
[9] K. G. Fissum *et al.*, Phys. Rev. **C 70**, 034606 (2004).
[10] D. Dutta *et al.*, Phys. Rev. **C 68**, 064603 (2003).
[11] P. Mergell, U.-G. Meissner, and D. Drechsel, Nucl. Phys. **A596**, 367 (1996).
[12] C. J. Horowitz and B. D. Serot, Nucl. Phys. **A368**, 503 (1986).
[13] M. M. Sharma, M. A. Nagarajan, and P. Ring, Phys. Lett. **B 312**, 377 (1993).
[14] E. D. Cooper, S. Hama, B. C. Clark, and R. L. Mercer, Phys. Rev. **C 47**, 297 (1993).
[15] G. R. Satchler, *Direct Nuclear Reactions* (Oxford University Press, N.Y., 1983).
[16] G. Rawitscher, Phys. Rev. **C 56**, 2029 (1997).
[17] H. S. Sherif, R. I. Sawafta, and E. D. Cooper, Nucl. Phys. **A449**, 708 (1986).

[18] C. J. Horowitz, D. P. Murdoch, and B. D. Serot, in *Computational Nuclear Physics I: Nuclear Structure*, edited by K. Langanke, J. A. Maruhn, and S. E. Koonin (Springer-Verlag, Berlin, 1991), pp. 129–151.
[19] J. J. Kelly, Adv. Nucl. Phys. **23**, 75 (1996).
[20] M. Hedayati–Poor, J. I. Johansson, and H. S. Sherif, Phys. Rev. **C 51**, 2044 (1995).
[21] J. M. Udías, P. Sarriguren, E. M. de Guerra, E. Garrido, and J. A. Caballero, Phys. Rev. **C 51**, 3246 (1995).
[22] F. Perey and B. Buck, Nucl. Phys. **32**, 353 (1962).
[23] Y. Jin and D. S. Onley, Phys. Rev. **C 50**, 377 (1994).
[24] C. M. Spaltro, H. P. Blok, E. Jans, L. Lapikás, M. van der Schaar, G. van der Steenhoven, and P. K. A. de Witt Huberts, Phys. Rev. **C 48**, 2385 (1993).
[25] L. Chinitz *et al.*, Phys. Rev. Lett. **67**, 568 (1991).
[26] J. J. Kelly, to be submitted to Phys. Rev. C (unpublished).
[27] G. van der Steenhoven, H. P. Blok, E. Jans, M. de Jong, L. Lapikás, E. N. M. Quint, and P. K. A. de Witt Huberts, Nucl. Phys. **A480**, 547 (1988).
[28] G. van der Steenhoven, H. P. Blok, E. Jans, L. Lapikás, E. N. M. Quint, and P. K. A. de Witt Huberts, Nucl. Phys. **A484**, 445 (1988).
[29] J. J. Kelly and S. J. Wallace, Phys. Rev. **C 49**, 1315 (1994).